


## Efficient Chiral-Domain-Wall Motion Driven by Spin-Orbit Torque in Metastable Platinum Films

Chirag Garg,<sup>1,\*</sup> See-Hun Yang,<sup>1,†,‡</sup> Leslie Thompson,<sup>1</sup> Teya Topuria<sup>Ⓢ</sup>,<sup>1</sup> Amir Capua,<sup>2</sup> Brian Hughes,<sup>1</sup> Timothy Phung,<sup>1</sup> Panagiotis Ch. Filippou,<sup>1</sup> and Stuart S.P. Parkin<sup>Ⓢ</sup><sup>1,3,§</sup>

<sup>1</sup>*IBM Research - Almaden, San Jose, California 95120, USA*

<sup>2</sup>*Department of Applied Physics, Hebrew University, 91904 Jerusalem, Israel*

<sup>3</sup>*Max Planck Institute for Microstructure Physics, 06120 Halle, Germany*

 (Received 21 February 2020; revised 20 July 2020; accepted 17 August 2020; published 21 September 2020)

The properties and characteristics of thin-film materials strongly depend on their textures and orientations. However, the attainable film morphologies are severely limited by substrates and growth thermodynamics. Metastable films that otherwise cannot be grown by conventional growth methods may overcome these limitations, thus allowing a dramatic expansion of the spectrum of film textures and orientations. Here we present a means to grow metastable platinum layers that are deposited from platinum alloyed with bismuth surfactant material. This is distinct from conventional surfactant-aided growth of films in which surfactants are typically deposited onto the substrate before film deposition, altering the film growth mode but not the film morphology by tuning the surface energy. Surprisingly, we find that almost no bismuth is incorporated into the platinum layer, but rather the structural morphology of this layer is significantly altered. When this metastable platinum layer is applied to spin-orbit-torque technology, a huge increase in the current-driven velocity of chiral domain walls in perpendicularly magnetized wire on top of the metastable platinum layer is observed for otherwise the same current density, while the platinum resistivity is found to barely increase. Our findings show that the metastable film grown from material alloyed with surfactant is promising for the development of devices in various fields, such as spintronics, semiconductors, and quantum materials.

DOI: [10.1103/PhysRevApplied.14.034052](https://doi.org/10.1103/PhysRevApplied.14.034052)

### I. INTRODUCTION

Surfactant-aided epitaxial film growth [1] has been widely used to improve film smoothness or control the growth mode. For example, smooth magnetic layers can be grown with use of surfactants such as Ag [2], In [3], Bi [4–6], and Pb [7,8], thus increasing giant magnetoresistance and exchange bias in spin valves, or semiconducting InAs islands on GaAs(110) can be grown with use of Bi surfactant to form self-assembled quantum dots for photoluminescence [9,10]. Surfactants are usually predeposited on a substrate to control the surface energy and growth kinetics before growth of films that are of interest, thus raising or lowering the surface energy of the substrate underneath. As the following layer is being deposited, the surfactants float out to the surface [Fig. 1(a)]. The increased substrate surface energy leads to a two-dimensional smooth layer (Frank–van der

Merwe mode), while the formation of three-dimensional islands is favored by the decreased substrate surface energy (Volmer-Weber or Stranski-Krastanov mode). This conventional surfactant-aided growth does not affect the structure and orientation of films, which are dictated by the crystal structure of the substrate underneath since the surfactants affect the growth mode only [Fig. 1(a)].

Here we show that when Pt-Bi films are sputter-deposited from a Pt<sub>85</sub>Bi<sub>15</sub>-alloy target, the deposited Pt-Bi films contain hardly any bismuth, thus forming pure Pt films covered with a very thin bismuth layer (approximately 3 Å) on top [see Fig. 1(b)]. This suggests that the bismuth behaves like a surfactant that typically floats out to the surface. However, most importantly we discover that the structural morphology of Pt-Bi film is significantly altered and it grows as a mixture of (111)- and (100)-oriented grains, whereas the Pt films deposited from a pure Pt target grow with a (111) orientation unless they are grown on substrates such as MgO [11,12] or Al<sub>2</sub>O<sub>3</sub> [13]. Hence, the Pt-Bi film grown from the Pt<sub>85</sub>Bi<sub>15</sub>-alloy target is metastable, forming a local minimum in structural phase, while the Pt(111) texture grown from the Pt target sits at a global minimum [Fig. 1(b)]. This is distinct

\*chiraggarg.in@outlook.com

†seehun@gmail.com

‡seeyang@us.ibm.com

§stuart.parkin@mpi-halle.mpg.de

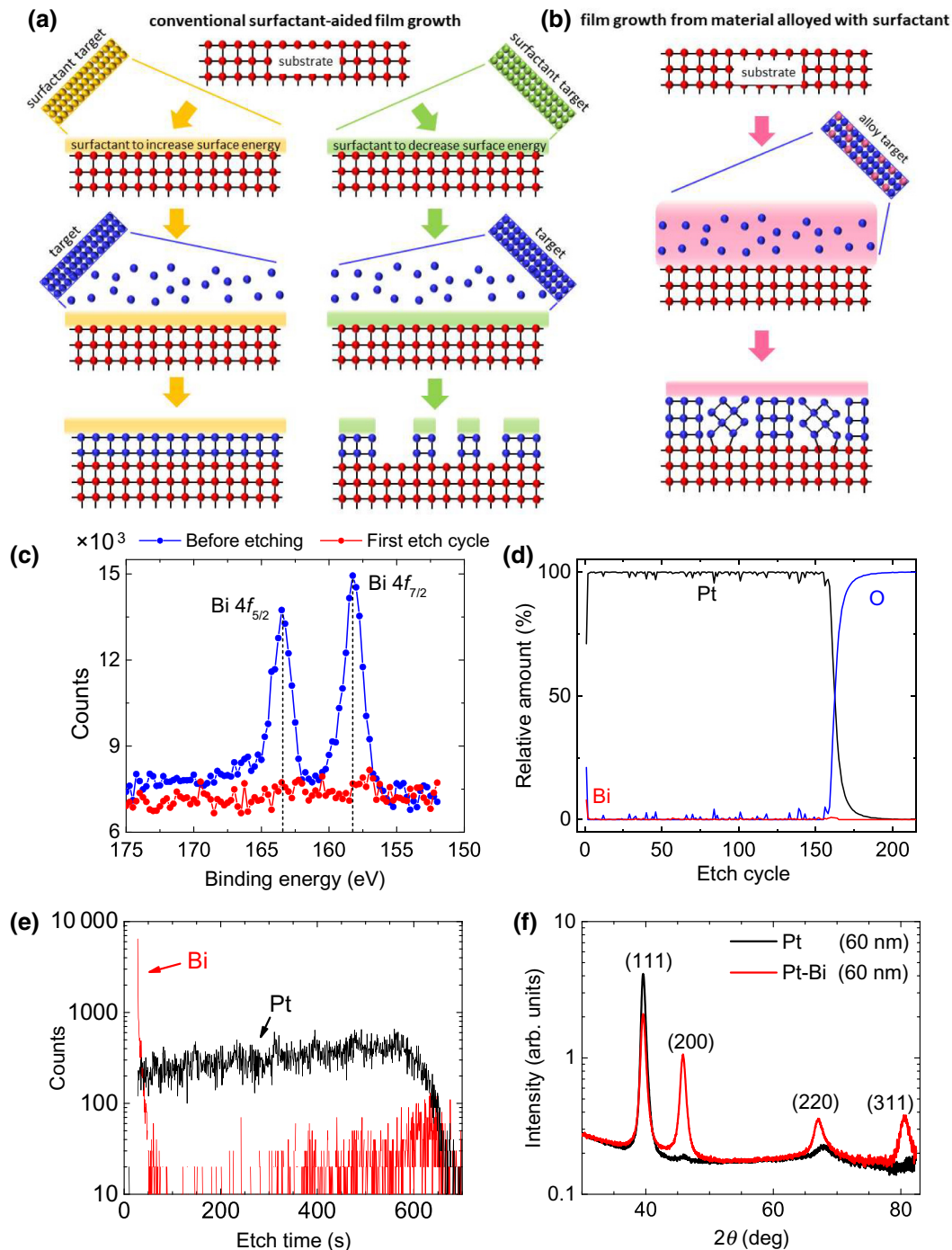


FIG. 1. Distinction between two film-growth methods using surfactants, and characterization of 60-nm-thick films grown from a  $\text{Pt}_{85}\text{Bi}_{15}$  target. Illustration of (a) conventional surfactant-aided film growth (left panel Frank–van der Merwe mode, right panel Volmer–Weber mode) and (b) film growth from materials alloyed with surfactants. Shaded areas correspond to surfactant materials, while blue circles represent material atoms that are of interest. (c) XPS spectrum of Bi  $4f$  orbitals obtained before etching and after one cycle of etching. (d) Relative concentration of the elements Pt, Bi, and O for various depths obtained by XPS. (e) Secondary-ion-mass-spectroscopy depth profile of Pt and Bi. (f) Comparison of XRD patterns obtained from films grown from a Pt target and a  $\text{Pt}_{85}\text{Bi}_{15}$  target.

from conventional surfactant-aided growth, which does not affect the crystal orientation but changes the surface energy only as discussed above [Figs. 1(a) and 1(b)].

As an application of this growth method, we incorporate the Pt-Bi film as a spin-orbit-torque (SOT) source into magnetic wires [14,15] on the basis of the current-induced

domain-wall (DW) motion (CIDWM) [16–20]. We find dramatically increased current-induced domain-wall velocities for otherwise the same current density for magnetic wires formed on Pt-Bi underlayers compared with Pt films grown from Pt targets containing no bismuth. Here amorphous Co-Gd and Ni-Gd magnetic multilayers are used in the magnetic wires, showing excellent perpendicular magnetic anisotropy on both Pt-Bi and Pt underlayers. We find that this remarkably efficient CIDWM can be accounted for by large spin currents generated from the metastable Pt film, and the spin currents are likely induced by the spin Hall effect (SHE), which is quantified by the spin Hall angle ( $\theta_{\text{SHE}}$ ), which details the conversion of charge current to spin current [21]. Our findings show that the method of growing metastable films has the potential to be used not only to dramatically increase figure of merits but also to allow more functionalities in various fields that otherwise are impossible by conventional means.

## II. GROWTH, MATERIAL, AND CHEMICAL CHARACTERIZATION

Various thin-film structures are prepared by dc magnetron sputtering in an ultrahigh-vacuum deposition system with a base pressure of  $10^{-9}$  Torr. The films are deposited at ambient temperature in 3-mTorr argon sputter gas. To characterize the properties of the Pt-Bi and Pt films, thick films (approximately 60 nm thick) are grown from both  $\text{Pt}_{85}\text{Bi}_{15}$  and pure Pt targets onto oxidized silicon substrates (i.e., onto amorphous  $\text{SiO}_2$ ). Their chemical composition is determined by Rutherford-backscattering (RBS) analysis. Surprisingly, the Pt-Bi films contain only trace amounts of Bi of approximately  $(1 \pm 0.5)\%$ , which is more than 1 order of magnitude below the composition of the sputtering target (as confirmed by RBS analysis). Since energy-dispersive-x-ray-spectroscopy measurements of these films are also not able to detect Bi within the detection limits of the instrument, we perform x-ray-photoelectron-spectroscopy (XPS) measurements to determine the detailed chemical composition of the film as a function of its depth, as shown in Figs. 1(c) and 1(d). Figure 1(c) shows the Bi  $4f$  peaks situated at 158.3 and 163.5 eV for the as-deposited sample. These values are shifted from those of metallic Bi, indicative of oxidation. The depth profile is acquired by etching in 30-s cycles with an Ar-ion source. The XPS spectrum after the first etch cycle shows no trace of Bi. Figure 1(d) plots the relative concentration of the elements Pt, Bi, and O as a function of the etch cycle. The Bi signal disappears after the first etch cycle, showing that Bi segregates to the surface and is not incorporated into the bulk of the film, within experimental error. The Pt signal is reduced to less than 1% of its initial intensity after 184 etch cycles, resulting in an average etch rate of approximately  $3.2 \text{ \AA}$  Pt per cycle. Thus, the only Bi that is incorporated in the film is about a

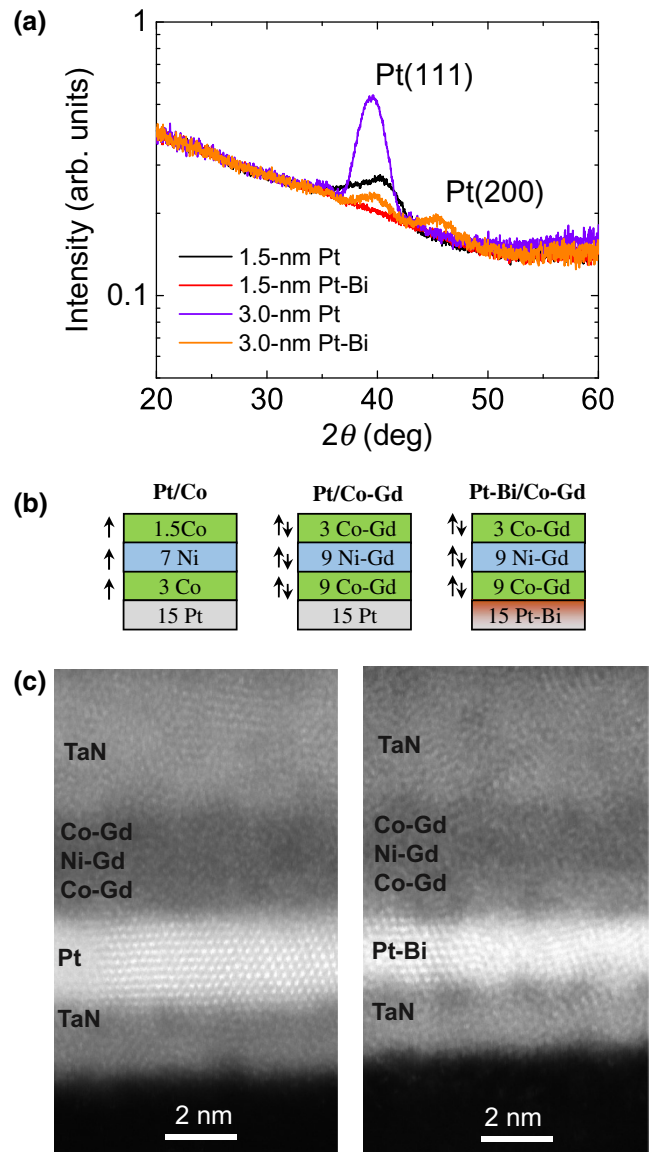


FIG. 2. Film stacks grown for SOT study. (a) XRD patterns obtained for thinner Pt and Pt-Bi films. (b) Details of the films grown for SOT study. These layers are grown on  $\text{AlO}_x(100 \text{ \AA})/\text{TaN}(20 \text{ \AA})$  and capped with  $\text{TaN}(50 \text{ \AA})$ . Numbers denote thickness in angstroms. (c) Cross-section STEM of Pt/Co-Gd (left) and Pt-Bi/Co-Gd (right) films.

monolayer (approximately  $3.08 \text{ \AA}$ ) despite a Bi concentration of 15% in the  $\text{Pt}_{85}\text{Bi}_{15}$  sputter target. The XPS results are consistent with the RBS results, which show a trace amount of Bi in the film. For further corroboration we use another analysis technique, secondary-ion mass spectroscopy, with similar conclusions to those of the XPS and RBS experiments [Fig. 1(e)].

Bi is a well-known surfactant [22–24], whereby it may segregate to the surface of a film during growth. If Bi

played a role as a conventional surfactant, it would influence growth modes only but not structures or orientations, as discussed above. However, on the contrary, we find from x-ray-diffraction (XRD) measurements that the structures of the Pt-Bi and Pt films are highly distinctive [Fig. 1(f)]. While the films grown from the Pt target are highly (111) crystalline oriented, the Pt-Bi films, by contrast, are poorly textured with significant amounts of both (111) and (100) orientations in the ratio 2:1. We also observe lesser amounts of (220) and (311) orientations. These results are surprising as Pt has a strong tendency to grow as (111), and growth of other orientations of Pt is usually accomplished by epitaxial growth on lattice-matched substrates. We find no bismuth XRD peaks from the Pt-Bi films, consistent with the absence of any significant Bi content from our previous characterizations. The difference in film morphology is reflected in a slightly increased resistivity of the Pt-Bi films (the resistivities of 60-nm-thick Pt-Bi and Pt films are  $21 \mu\Omega \text{ cm}$  and  $18 \mu\Omega \text{ cm}$ , respectively). Since Bi is present only at the surface of the Pt-Bi films, we attribute this increased resistivity to the polycrystalline nature of Pt-Bi. XRD and STEM scans of thinner films [see Figs. 2(a) and 2(c) and Supplemental Material [25]] reveal similar differences in structure as seen in the 60-nm-thick films, although the peaks are broader due to the smaller grain sizes. These findings are in sharp contrast with conventional surfactant-aided growth.

The modification of structural properties was previously shown to greatly increase the spin Hall angle and associated SOTs generated in thin films of metals such as Pt [26–28], Ta [29], and W [30,31]. To test the strength of SOT generated from metastable Pt, we fabricate perpendicularly magnetized magnetic wires from  $\text{AlO}_x(100 \text{ \AA})/\text{TaN}(20 \text{ \AA})/\text{Pt}$  or  $\text{Pt-Bi}(15 \text{ \AA})/\text{Co-Gd}(9 \text{ \AA})/\text{Ni-Gd}(9 \text{ \AA})/\text{Co-Gd}(3 \text{ \AA})/\text{TaN}(50 \text{ \AA})$  multilayered structures that are deposited on silicon substrates capped with a 25-nm-thick silicon oxide layer. All thicknesses unless specified are in angstroms. In our earlier work [18], the growth of a magnetic trilayer composed of Co/Ni/Co on Pt(111) layers induced a strong perpendicular magnetic anisotropy (PMA) as well as the formation of Néel DWs stabilized through a Dzyaloshinsky-Moriya interaction (DMI) [32,33]. These DWs can be driven by current at high speeds by use of SOT. We find that, in comparison with the Pt/Co interface, the Pt-Bi/Co interface does not have sufficient interfacial anisotropy to induce PMA in Co/Ni/Co layers. This likely arises from the strong dependence of the interfacial magnetic anisotropy in these layers on the (111) orientation of the Pt film [34]. However, we find that by replacing the Co/Ni/Co ferromagnetic trilayer with a ferrimagnetic trilayer made of Co-Gd/Ni-Gd/Co-Gd, PMA films can be formed on Pt-Bi underlayers. The Co-Gd and Ni-Gd films are grown with use of alloy sputter targets. The compositions of the films [Co ( $75.3 \pm 0.5\%$ ) and Gd ( $24.7 \pm 0.5\%$ ); Ni ( $86.4 \pm 0.5\%$ ) and Gd ( $13.6 \pm 0.5\%$ ),

as determined by RBS, are very close to those of the targets, in contrast to the case of the Pt-Bi films.

Films of rare-earth–transition-metal alloys, such as Co-Gd or Ni-Gd films, exhibit a bulk perpendicular anisotropy [35]. Moreover, the compensated moments resulting from the antiferromagnetic ordering between the  $3d$ -transition-metal and  $4f$ -rare-earth moments reduces the shape anisotropy that needs to be overcome to induce PMA. Three distinct films stacks (Pt/Co, Pt/Co-Gd, and Pt-Bi/Co-Gd) are used for our SOT studies, whose structures and the corresponding labels that we use to describe them are shown in Fig. 2(b). Cross-section STEM images for Pt/Co-Gd and Pt-Bi/Co-Gd show that the ferrimagnetic layers are amorphous for both underlayers and confirm that the Pt layer is highly (111) textured in contrast to Pt-Bi, which has a mixed texture [Fig. 2(c)].

### III. DOMAIN-WALL MOTION RESULTS

CIDWM was studied in the three film stacks by patterning them into nanowire devices of size  $50 \times 2 \mu\text{m}^2$ . A typical device studied for CIDWM is shown in Fig. 3(a) (see the inset). Domain-wall displacements in the nanowire were imaged by Kerr microscopy in differential mode. Current pulse lengths ranging from a few nanoseconds to 1 ns are used to capture the dependence on domain-wall velocity,  $v$ , and on current density in the underlayer  $J_{\text{UL}}$  as shown in Figs. 3(a) and 3(b). To calculate  $J_{\text{UL}}$ , the conductance of the stack deposited without the underlayer ( $G^*$ ) is subtracted from the conductance of the complete stack ( $G$ ), such that  $J_{\text{UL}} = 2V/(R + 50)[(G - G^*)/G](1/A)$ , where  $R$  is the resistance of the device and  $A$  is the cross-section area of the underlayer. The factor of 2 in this equation is because the voltage along the nanowire is twice the source voltage due to the impedance mismatch between the nanowire and the source. We define  $J_C$  to be the threshold current density in the underlayer at which CIDWM is observed with pulses that are less than 100 ns long. For all three stacks, we find  $v$  at  $J_C$  to be greater than 5 m/s. However, we find significant differences between the three stacks, with much lower values of  $J_C$  for Pt-Bi/Co-Gd as compared with the other two stacks.  $J_C$  for Pt/Co-Gd is about half that for Pt/Co. Moreover, the DW velocities in Pt-Bi/Co-Gd nanowires are much greater than those in Pt/Co-Gd for the same  $J_{\text{UL}}$ . In particular, the DWs in Pt-Bi/Co-Gd reach a velocity of approximately 250 m/s around the  $J_C$  for Pt/Co. The lowest  $J_C$  ( $6 \text{ MA/cm}^2$ ), which we find in Pt-Bi/Co-Gd, is comparable to an earlier result in ferrimagnetic Heusler systems [36] but is much lower than reported results on ferromagnetic systems [18,37]. Thus, in summary, we find that the  $v$ -versus- $J_{\text{UL}}$  characteristics of the Pt-Bi/Co-Gd ferrimagnetic system are much improved over those of the Pt/Co ferromagnetic system.

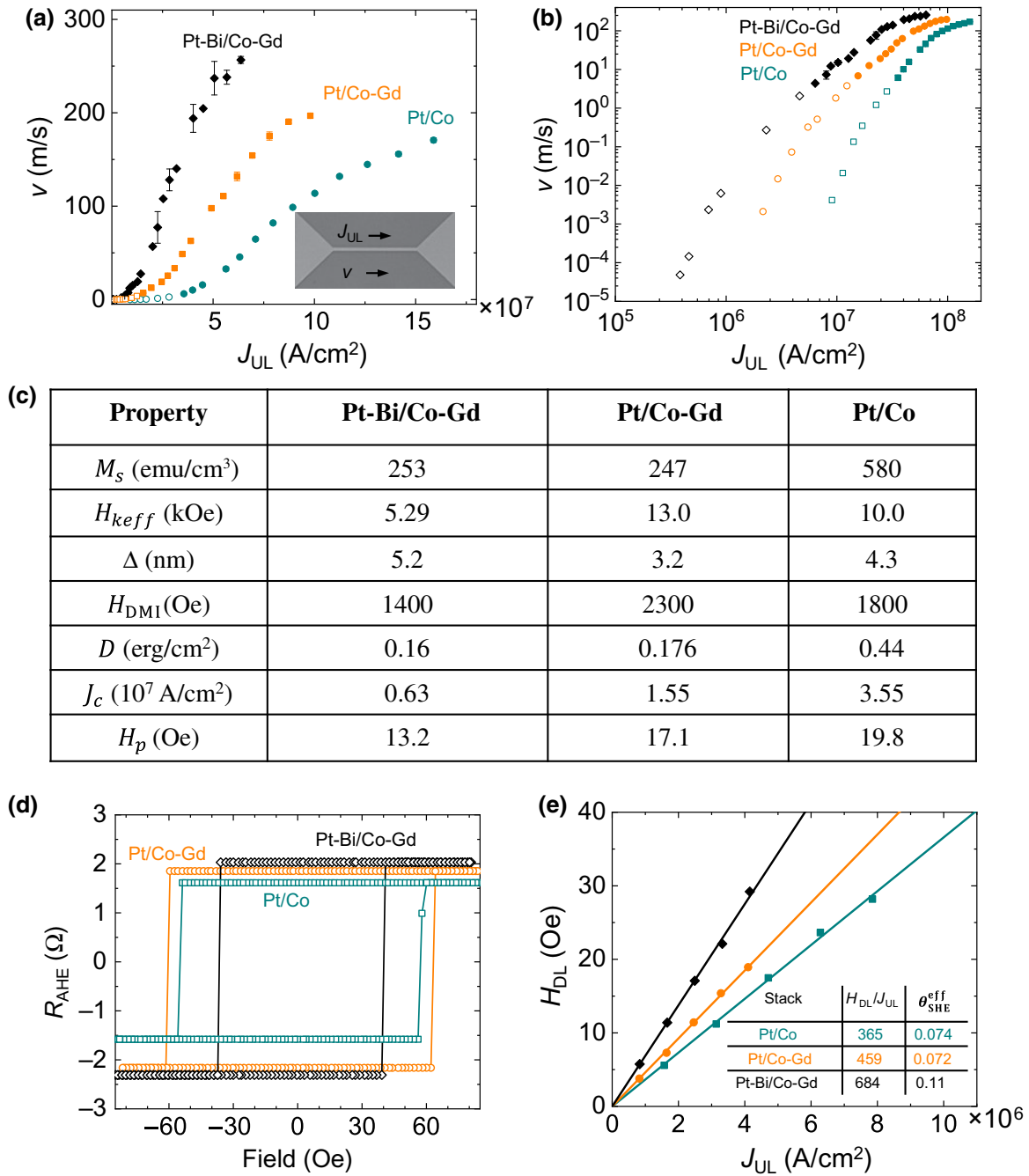


FIG. 3. Magnetics, current-driven domain-wall motion, and SOT for Pt-Bi/Co-Gd, Pt/Co-Gd, and Pt/Co. (a),(b)  $v$  versus  $J_{UL}$  in (a) linear-linear (a) and (b) log-log representation. Solid symbols indicate use of pulse lengths up to 100 ns. Hollow symbols indicate use of pulse lengths greater than 100 ns. (c) Summary of parameters obtained by experiments as well as modelling. (see Supplemental Material [25] for more details).  $H_{keff}$  refers to effective anisotropy field. (d) Hysteresis loops of Hall resistance ( $R_{AHE}$ ) obtained by application of an out-of-plane magnetic field. (e) Quantification of the dampinglike effective field ( $H_{DL}$ ) by second-harmonic Hall measurements. All measurements are performed at room temperature.

The strength of the DMI induced at the underlayer-magnetic-layer interface of each stack is determined by exploring the dependence of the CIDWM on the longitudinal magnetic field ( $H_x$ ) [18,37]. As the magnitude of  $H_x$  becomes equal and opposite in sign to that of the internal

DMI field ( $H_{DMI}$ ) acting on the Néel domain walls, the DW reverts to a Bloch configuration, resulting in the absence of any CIDWM. The measurement data are fit to a well-established one-dimensional analytical model with use of experimentally obtained parameters and fitting parameters

(see Supplemental Material [25] for more details). From this analysis, the DMI constant,  $D$ , can be obtained from  $D = H_{\text{DMI}} M_S \sqrt{A/K_{\text{eff}}}$ , where  $M_S$  is the magnetization of the film,  $K_{\text{eff}}$  is the effective anisotropy energy, and  $A$  is the exchange stiffness.  $\Delta$ , the domain-wall width parameter, is defined as  $\sqrt{A/K_{\text{eff}}}$ . The parameters thereby obtained are summarized in the table in Fig. 3(c). As discussed earlier, the polycrystalline nature of Pt-Bi/Co-Gd leads to a smaller  $K_{\text{eff}}$  (0.67 Merg/cm<sup>3</sup>) as compared with Pt/Co-Gd (1.60 Merg/cm<sup>3</sup>). The Pt-Bi/Co-Gd and Pt/Co-Gd stacks both have similar magnitudes of  $D$ , suggesting that the magnitude of  $D$  is not much influenced by either the orientation of the Pt grains or the presence of Bi atoms at the interface. However, the magnitude of  $D$  for the ferrimagnetic samples is less than half that of Pt/Co which is likely related to the lower magnetization of Co-Gd compared with Co.

Out-of-plane anomalous-Hall-effect (AHE) measurements of the three stacks are compared in Fig. 3(d). The magnitude and sign of the AHE are similar in all three cases, but the coercivity is smaller for the Pt-Bi/Co-Gd stack, likely due to the smaller DW nucleation field. The similar magnitude of the AHE suggests that for the ferrimagnetic samples, the contribution from the Co sublattice is dominant compared with that from the Gd sublattice.

To probe the origin of the faster CIDWM in Pt-Bi/Co-Gd, harmonic-Hall-voltage measurements [38,39] are performed to quantify the dampinglike ( $H_{\text{DL}}$ ) and fieldlike effective fields ( $H_{\text{FL}}$ ). These measurements are performed by probing the first-harmonic and second-harmonic Hall voltage signals under the application of magnetic fields applied in the plane either longitudinal or transverse to the direction of the current (more details are given in Supplemental Material [25]). Most importantly, we find that there is an approximately 52% increase in the  $H_{\text{DL}}$  values for the Pt-Bi/Co-Gd sample as compared with the Pt/Co-Gd sample, as seen in Fig. 3(e). One possibility to account for the increased  $H_{\text{DL}}$  is the enhanced transparency of the Pt-Bi/Co-Gd interface. Because of the transparency [27,40],  $T$ , at the interface between the underlayer and the magnetic layer, the amount of spin current diffusing into the magnetic layer is lower than expected from the intrinsic spin Hall angle ( $\theta_{\text{SHE}}$ ) of the underlayer, such that the effective spin Hall angle acting in the magnetic layer,  $\theta_{\text{SHE}}^{\text{eff}}$ , is  $\theta_{\text{SHE}} T$ . It is then reasonable to assume that the transparency of the Pt-Bi/Co-Gd interface might be affected by any Bi segregated at this interface or by the polycrystalline nature of the Pt-Bi layer. Any change in transparency is reflected by an increase or decrease in the spin pumping, which can be measured through damping measurements. Thus, the intrinsic Gilbert damping values,  $\alpha$ , are obtained by studying the dynamical properties of the films using a pump-probe time-resolved magneto-optical-Kerr-effect [41] method (see Supplemental Material [25]). From these studies  $\alpha$  is determined to be approximately 0.105 for

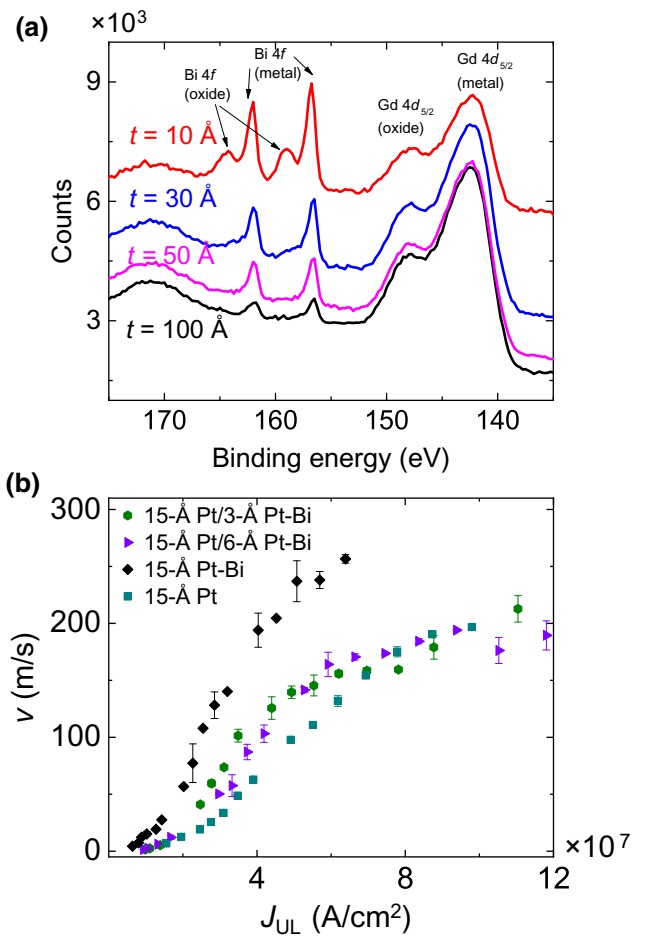


FIG. 4. Characterization of Bi segregation and its effect on current-driven domain-wall motion. (a) XPS spectra of Pt-Bi(45 Å)/Co-Gd( $t$ ) films grown on Si substrates. (b)  $v$  versus  $J_{\text{UL}}$  for various SOT stacks with the Co-Gd/Ni-Gd/Co-Gd trilayer but different underlayers.

Pt-Bi/Co-Gd and approximately 0.155 for Pt/Co-Gd. The lower  $\alpha$  of the Pt-Bi/Co-Gd stack implies that the spin-mixing conductance is decreased at this interface, with, consequently, lower transparency of this interface. Thus, the higher  $\theta_{\text{SHE}}^{\text{eff}}$  for this system cannot be accounted for by increased transparency of this interface, but rather the magnitude of the intrinsic spin Hall effect is greater for Pt-Bi.

Next, the source of increased SOT in Pt-Bi/Co-Gd is examined. The Pt/Co-Gd and Pt-Bi/Co-Gd stacks are identical except for the Pt underlayer. The enhanced SOT may have either a bulk origin from the growth of differently oriented Pt grains or an interfacial origin from any presence of Bi [42,43] at the Pt-Bi/Co-Gd interface. As discussed above, it is clear that Bi segregates to the top of a Pt-Bi film, but whether it continues that process once a Co-Gd film is grown on top of it needs to be determined. Thus, films of the form Pt-Bi(45 Å)/Co-Gd( $t$ ) are prepared with differing  $t$  as shown in Fig. 4(a). If the Bi continues

floating out for Co-Gd, the strength of the Bi XPS spectrum would remain unchanged as a function of  $t$ . If instead Bi remains segregated at the Pt-Bi/Co-Gd interface, then the signal should vanish with increasing  $t$ . The latter is found [Fig. 4(a)], and at  $t=100$  Å, the signal has nearly vanished. Evidence of oxidation of the Bi for  $t=10$  Å is again consistent with the Bi remaining at the Pt-Bi/Co-Gd interface.

Having shown that Bi is confined to the Pt-Bi/Co-Gd interface, we perform further experiments to probe the origin of the SOT. Additional film stacks in which a thin layer of Pt-Bi (3 and 6 Å) is inserted between Pt and Co-Gd are prepared. If the origin of the increased SOT is solely from the introduction of bismuth at the interface, then a thin layer should suffice for replicating our earlier results with Pt-Bi/Co-Gd. The CIDWM results for these samples are overlaid with our earlier results in Fig. 4(b). The introduction of a Pt-Bi insertion layer increases the speed of the DWs but this still noticeably lags behind that of the Pt-Bi/Co-Gd sample. Thus, these results show that instead the modified structure of the Pt layer likely plays a significant role.

A linear scaling between the resistivity and the spin Hall angle of the Pt-Bi underlayer would imply that the increased SOT is governed by the Elliot-Yafet mechanism [44,45]. However, the increase in the spin Hall angle is much greater than the increase in the resistivity, so we rule out this possibility. This would be rather consistent with Dyakonov-Perel scattering in crystalline Pt thin films [46,47] and would lead to different spin-dependent scattering in differently oriented grains.

#### IV. CONCLUSION

We find that bismuth introduced via a Pt-Bi-alloy sputtering target changes the structure of the Pt film while floating out to the surface, distinct from conventional surfactant-aided growth. This metastable Pt film dramatically increases spin-orbit scattering, which gives rise to a strongly increased spin Hall effect without a comparable increase in resistivity. Film growth from materials alloyed with surfactants is a means of providing increased spin-orbit torques without increases in resistivity and is therefore technologically very relevant, and can be extended to other areas such as semiconductors and quantum matters.

#### ACKNOWLEDGMENTS

We thank the Army Research Office (Contract No. W911NF-13-1-0107) for its partial support of this work. We thank Andrew Kellock and Eugene Delenia for their help.

[1] M. Copel, M. C. Reuter, E. Kaxiras, and R. M. Tromp, Surfactants in Epitaxial Growth, *Phys. Rev. Lett.* **63**, 632 (1989).

[2] H. D. Chopra, D. X. Yang, P. J. Chen, and W. F. Egelhoff, Surfactant-Assisted atomic-level engineering of spin valves, *Phys. Rev. B* **65**, 094433 (2002).

[3] W. F. Egelhoff, P. J. Chen, C. J. Powell, M. D. Stiles, and R. D. McMichael, Growth of giant magnetoresistance spin valves using indium as a surfactant, *J. Appl. Phys.* **79**, 2491 (1996).

[4] M. Kamiko, A. Nakamura, K. Aotani, and R. Yamamoto, Bi surfactant effects of Co/Cu multilayered films prepared by sputter deposition, *Appl. Surf. Sci.* **256**, 1257 (2009).

[5] M. Kamiko, H. Mizuno, H. Chihaya, R. Yamamoto, J. Xu, and I. Kojima, Enhancement in layer-by-layer growth in heteroepitaxial growth of Co on Au(111) surface by Bi surfactant, *J. Appl. Phys.* **100**, 113532 (2006).

[6] M. Kamiko, H. Mizuno, H. Chihaya, J. Xu, I. Kojima, and R. Yamamoto, Effect of Bi surfactant on the heteroepitaxial growth in Fe/Cr(100) multilayers, *Solid State Commun.* **134**, 803 (2005).

[7] J. Camarero, L. Spendeler, G. Schmidt, K. Heinz, J. J. de Miguel, and R. Miranda, Surfactant-Induced Suppression of Twin Formation During Growth of Fcc Co/Cu Superlattices on Cu(111), *Phys. Rev. Lett.* **73**, 2448 (1994).

[8] W. F. Egelhoff, P. J. Chen, C. J. Powell, M. D. Stiles, R. D. McMichael, C.-L. Lin, J. M. Sivertsen, J. H. Judy, K. Takano, and A. E. Berkowitz, Growth of giant magnetoresistance spin valves using Pb and Au as surfactants, *J. Appl. Phys.* **80**, 5183 (1996).

[9] R. B. Lewis, P. Corfdir, H. Li, J. Herranz, C. Pfüller, O. Brandt, and L. Geelhaar, Quantum Dot Self-Assembly Driven by a Surfactant-Induced Morphological Instability, *Phys. Rev. Lett.* **119**, 086101 (2017).

[10] R. B. Lewis, A. Trampert, E. Luna, J. Herranz, C. Pfüller, and L. Geelhaar, Bismuth-Surfactant-Induced growth and structure of InAs/GaAs(110) quantum dots, *Semicond. Sci. Technol.* **34**, 105016 (2019).

[11] K. H. Ahn, S. Baik, and S. S. Kim, Change of growth orientation in Pt films epitaxially grown on MgO(001) substrates by sputtering, *J. Mater. Res.* **17**, 2334 (2002).

[12] P. C. McIntyre, C. J. Maggiore, and M. Nastasi, Orientation selection in thin platinum films on (001) MgO, *J. Appl. Phys.* **77**, 6201 (1995).

[13] A. J. Francis, Y. Cao, and P. A. Salvador, Epitaxial growth of Cu(100) and Pt(100) thin films on perovskite substrates, *Thin Solid Films* **496**, 317 (2006).

[14] S. S. P. Parkin, M. Hayashi, and L. Thomas, Magnetic domain-wall racetrack memory, *Science* **320**, 190 (2008).

[15] S. Parkin and S.-H. Yang, Memory on the racetrack, *Nat. Nanotechnol.* **10**, 195 (2015).

[16] M. Hayashi, L. Thomas, R. Moriya, C. Rettner, and S. S. P. Parkin, Current-Controlled magnetic domain-wall nanowire shift register, *Science* **320**, 209 (2008).

[17] I. M. Miron, T. Moore, H. Szambolics, L. D. Buda-Prejbeanu, S. Auffret, B. Rodmacq, S. Pizzini, J. Vogel, M. Bonfim, A. Schuhl, and G. Gaudin, Fast current-induced domain-wall motion controlled by the rashba effect, *Nature Mater* **10**, 419 (2011).

[18] K.-S. Ryu, L. Thomas, S.-H. Yang, and S. Parkin, Chiral spin torque at magnetic domain walls, *Nat. Nanotechnol.* **8**, 527 (2013).

- [19] S. Emori, U. Bauer, S.-M. Ahn, E. Martinez, and G. S. D. Beach, Current-Driven dynamics of chiral ferromagnetic domain walls, *Nat. Mater.* **12**, 611 (2013).
- [20] S.-H. Yang, K.-S. Ryu, and S. Parkin, Domain-Wall velocities of up to  $750 \text{ m s}^{-1}$  driven by exchange-coupling torque in synthetic antiferromagnets, *Nat. Nanotechnol.* **10**, 221 (2015).
- [21] A. Hoffmann, Spin hall effects in metals, *IEEE Trans. Magn.* **49**, 5172 (2013).
- [22] A. Kawano, I. Konomi, H. Azuma, T. Hioki, and S. Noda, Influence of bismuth as a surfactant on the growth of germanium on silicon, *J. Appl. Phys.* **74**, 4265 (1993).
- [23] M. Marszałek, A. Polit, V. Tokman, Y. Zabala, and I. Protzenko, The effect of surfactants on the growth of Co/Cu multilayers, *Surf. Sci.* **601**, 4454 (2007).
- [24] S. Tixier, M. Adamcyk, E. C. Young, J. H. Schmid, and T. Tiedje, Surfactant enhanced growth of GaNAs and InGaNAs using bismuth, *J. Cryst. Growth* **251**, 449 (2003).
- [25] See Supplemental Material at <http://link.aps.org/supplemental/10.1103/PhysRevApplied.14.034052> for details of the one-dimensional model and other experiments.
- [26] L. Liu, T. Moriyama, D. C. Ralph, and R. A. Buhrman, Spin-Torque Ferromagnetic Resonance Induced by the Spin Hall Effect, *Phys. Rev. Lett.* **106**, 036601 (2011).
- [27] W. Zhang, W. Han, X. Jiang, S.-H. Yang, and S. S. P. Parkin, Role of transparency of platinum–ferromagnet interfaces in determining the intrinsic magnitude of the spin hall effect, *Nat. Phys.* **11**, 496 (2015).
- [28] M.-H. Nguyen, D. C. Ralph, and R. A. Buhrman, Spin Torque Study of the Spin Hall Conductivity and Spin Diffusion Length in Platinum Thin Films with Varying Resistivity, *Phys. Rev. Lett.* **116**, 126601 (2016).
- [29] L. Liu, C.-F. Pai, Y. Li, H. W. Tseng, D. C. Ralph, and R. A. Buhrman, Spin-Torque switching with the giant spin hall effect of tantalum, *Science* **336**, 555 (2012).
- [30] K.-U. Demasius, T. Phung, W. Zhang, B. P. Hughes, S.-H. Yang, A. Kellock, W. Han, A. Pushp, and S. S. P. Parkin, Enhanced spin–orbit torques by oxygen incorporation in tungsten films, *Nat Commun.* **7**, 1 (2016).
- [31] C.-F. Pai, L. Liu, Y. Li, H. W. Tseng, D. C. Ralph, and R. A. Buhrman, Spin transfer torque devices utilizing the giant spin hall effect of tungsten, *Appl. Phys. Lett.* **101**, 122404 (2012).
- [32] I. Dzyaloshinsky, A thermodynamic theory of “weak” ferromagnetism of antiferromagnetics, *J. Phys. Chem. Solids* **4**, 241 (1958).
- [33] T. Moriya, Anisotropic superexchange interaction and weak ferromagnetism, *Phys. Rev.* **120**, 91 (1960).
- [34] S. Oikawa, Y. Kato, S. Iwata, and S. Tsunashima, Enhanced In-plane magnetic anisotropies of ultrathin Pt/Co/Pt films, *J. Magn. Magn. Mater.* **165**, 394 (1997).
- [35] P. Hansen, C. Clausen, G. Much, M. Rosenkranz, and K. Witter, Magnetic and magneto-optical properties of rare-earth transition-metal alloys containing Gd, Tb, Fe, Co, *J. Appl. Phys.* **66**, 756 (1989).
- [36] P. C. Filippou, J. Jeong, Y. Ferrante, S.-H. Yang, T. Topuria, M. G. Samant, and S. S. P. Parkin, Chiral domain wall motion in unit-cell thick perpendicularly magnetized heusler films prepared by chemical templating, *Nat Commun.* **9**, 1 (2018).
- [37] K.-S. Ryu, S.-H. Yang, L. Thomas, and S. S. P. Parkin, Chiral spin torque arising from proximity-induced magnetization, *Nat. Commun.* **5**, 3910 (2014).
- [38] J. Kim, J. Sinha, M. Hayashi, M. Yamanouchi, S. Fukami, T. Suzuki, S. Mitani, and H. Ohno, Layer thickness dependence of the current-induced effective field vector in TaCoFeBMgO, *Nat. Mater.* **12**, 240 (2013).
- [39] M. Hayashi, J. Kim, M. Yamanouchi, and H. Ohno, Quantitative characterization of the spin-orbit torque using harmonic hall voltage measurements, *Phys. Rev. B* **89**, 144425 (2014).
- [40] C.-F. Pai, Y. Ou, L. H. Vilela-Leão, D. C. Ralph, and R. A. Buhrman, Dependence of the efficiency of spin hall torque on the transparency of Pt/ferromagnetic layer interfaces, *Phys. Rev. B* **92**, 064426 (2015).
- [41] A. Capua, S. Yang, T. Phung, and S. S. P. Parkin, Determination of intrinsic damping of perpendicularly magnetized ultrathin films from time-resolved precessional magnetization measurements, *Phys. Rev. B* **92**, 224402 (2015).
- [42] J. C. R. Sánchez, L. Vila, G. Desfonds, S. Gambarelli, J. P. Attané, J. M. D. Teresa, C. Magén, and A. Fert, Spin-to-Charge conversion using rashba coupling at the interface between Non-magnetic materials, *Nat. Commun.* **4**, 1 (2013).
- [43] S. Sangiao, J. M. De Teresa, L. Morellon, I. Lucas, M. C. Martinez-Velarte, and M. Viret, Control of the spin to charge conversion using the inverse rashba-edelstein effect, *Appl. Phys. Lett.* **106**, 172403 (2015).
- [44] R. J. Elliott, Theory of the effect of spin-orbit coupling on magnetic resonance in some semiconductors, *Phys. Rev.* **96**, 266 (1954).
- [45] Y. Yafet, in *Solid State Physics*, edited by F. Seitz, D. Turnbull (Academic, New York, 1963) Vols. 14.
- [46] J. Ryu, M. Kohda, and J. Nitta, Observation of the D’yakonov-Perel’ Spin Relaxation in Single-Crystalline Pt Thin Films, *Phys. Rev. Lett.* **116**, 256802 (2016).
- [47] R. Freeman, A. Zholud, Z. Dun, H. Zhou, and S. Urazhdin, Evidence for Dyakonov-Perel-Like Spin Relaxation in Pt, *Phys. Rev. Lett.* **120**, 067204 (2018).